Intensity and wavelength dependence of bimolecular recombination in P3HT:PCBM solar cells: A white-light biased external quantum efficiency study

Sarah R. Cowan, Jian Wang, Juan Yi, Yun-Ju Lee, Dana C. Olson et al.

Intensity and wavelength dependence of bimolecular recombination in P3HT:PCBM solar cells: A white-light biased external quantum efficiency study

Sarah R. Cowan,[1] Jian Wang,[2] Juan Yi,[3] Yun-Ju Lee,[2] Dana C. Olson,[1] and Julia W. P. Hsu[2,a)]

[1]*National Renewable Energy Laboratory, Golden, Colorado 80401, USA*
[2]*Department of Materials Science and Engineering, University of Texas at Dallas, Richardson, Texas 75080, USA*
[3]*Department of Physics, University of Texas at Dallas, Richardson, Texas 75080, USA*

Bimolecular recombination is often a major photogenerated charge carrier loss mechanism in organic photovoltaic (OPV) devices, resulting in lower fill factor (*FF*) compared to inorganic devices. The recombination parameter α can be obtained from the power law fitting of short-circuit current (J_{sc}) on illumination intensity (I), $J_{sc} \propto I^{\alpha}$, with α values less than unity taken as an indication of reduced photon-to-electron extraction efficiency and the presence of bimolecular recombination in OPV. Here, we show that this intensity-averaged measurement is inadequate. An external quantum efficiency (EQE) apparatus under constant white-light bias can be used to measure the recombination parameter (α_{EQE*}) as a function of wavelength and carrier density (white-light intensity). Examining the dependence of α on background white-light bias intensity and excitation wavelength provides further understanding of photon-to-electron conversion loss mechanisms in P3HT:PCBM bulk heterojunction devices in standard and inverted architectures. In order to compare EQE and current-voltage (*JV*) measurements, we discuss the special case of devices exhibiting sub-linear intensity response ($\alpha < 1$). Furthermore, we demonstrate several important advantages of the white-light biased EQE method of measuring bimolecular recombination compared to existing methods, including sensitivity in probing intensity-dependent recombination compared to steady-state *JV* measurements, the correlation of α_{EQE*} and *FF* in devices, elucidation of recombination mechanisms through spectral dependence of carrier loss, and the robustness of α_{EQE*} obtained via integration over the entire absorption region. Furthermore, this technique for measuring recombination is immediately accessible to the vast majority of researchers as the EQE apparatus is ubiquitous in PV research laboratories. © *2013 AIP Publishing LLC*
[http://dx.doi.org/10.1063/1.4801920]

I. INTRODUCTION

Organic photovoltaic (OPV) devices often have a lower fill factor (*FF*) than inorganic semiconductor solar cells. Bimolecular recombination of photogenerated charge carriers[1,2] as a result of unbalanced mobility,[1,3,4] energetic disorder,[5,6] high carrier density,[7] and/or space-charge limited (SCL) photocurrent[3,8] has been identified as a major loss mechanism and a cause of reduced *FF* in organic solar cells. Bimolecular recombination has been measured by many experimental techniques, including modeling of intensity-dependent current density-voltage (*JV*) data,[1–3,8] transient absorption spectroscopy,[9] photo-induced charge extraction by linearly increasing voltage,[10,11] and time-of-flight measurement of charge extraction.[12,13] In particular, the recombination parameter α can be obtained from the power law dependence of short-circuit current (J_{sc}) on illumination intensity (I), $J_{sc} \propto I^{\alpha}$, and α values less than unity have been taken as an indication of reduced photon-to-electron

conversion efficiency and the presence of bimolecular recombination.[1,3,8,14–18] Specifically, an α value of 0.5 has been interpreted as a signal of a device dominated by bimolecular recombination. However, for most devices, α determined from this method does not correlate strongly with device performance and does not deviate appreciably from unity even for low performance and low *FF* devices. In addition, α determined from $J_{sc} \propto I^{\alpha}$ is an average value over the intensity range in the measurement, while bimolecular recombination is dependent upon carrier density.

In *JV* measurements, recombination dynamics can also be probed via the intensity dependence of photocurrent at different voltage biases. As the applied voltage approaches open-circuit voltage (V_{oc}), i.e., reduced internal electric field gradient to collect carriers, bimolecular recombination effects become more prominent.[3,8] However, the exact value of α depends on the choice of voltage. In a different approach, Koster *et al.* measured the photocurrent due to a modulated photoexcitation at a single wavelength as a function of background illumination at the same wavelength and showed that such a method can more sensitively measure bimolecular recombination as a function of illumination

a)Author to whom correspondence should be addressed. Electronic mail: jwhsu@utdallas.edu

intensity (carrier density) and correlate it to device performance.[18] Here, we show that such a full-spectrum measurements of bimolecular recombination can be performed using an external quantum efficiency (EQE) apparatus under a white-light bias, and demonstrate advantages of the technique by quantifying recombination and the resulting effect on *FF* and overall device performance in inverted poly (3-hexylthiophene):[6,6]-phenyl C61-butyric acid methyl ester (P3HT:PCBM) organic photovoltaic devices with varying active layer thickness, as compared to analysis via steady-state *JV* measurements. The dependence of α on background white-light bias intensity and excitation wavelength provides further detailed understanding of intensity- and spectrally dependent photon-to-electron conversion loss mechanisms.

We demonstrate several important advantages of this approach, including increased sensitivity in probing intensity-dependent recombination compared to steady-state *JV* measurements, correlation between the EQE-measured recombination parameter and *FF* in devices, elucidation of recombination mechanisms through spectral dependence of carrier loss, and the robustness of the recombination parameter obtained via integration over the entire absorption region. Furthermore, our technique for measurement of recombination is immediately accessible to the vast majority of researchers as the EQE apparatus is ubiquitous in PV research laboratories.

In Sec. II of the paper, we describe the fabrication of P3HT:PCBM solar cells, intensity-dependent *JV* measurements with a solar simulator, apparatus for white-light biased EQE measurements, and calculation of carrier generation profile using one-dimensional (1D) transfer matrix method (TMM);[19,20] Sec. III discusses determination of photocurrent responsivity when intensity-dependence of photocurrent is non-linear; Sec. IV details determination of the bimolecular recombination parameter from white-light biased EQE data. The impact of active layer thickness in inverted P3HT:PCBM solar cells on bimolecular recombination is discussed in Sec. V, and spectral dependence of the bimolecular recombination parameter is found to be related to spatially dependent optical absorption in Sec. VI. Finally, a summary and the impact of this work are presented in Sec. VII. Additional materials are given in supplementary material.[21]

II. EXPERIMENTAL DETAILS

A. P3HT:PCBM solar cells

For inverted organic photovoltaic devices, patterned indium tin oxide (ITO) coated glass substrates (20 Ω/sq, Thin Film Devices) were first cleaned using ultrasonication in solutions of 1% volume aqueous surfactant solution (Aquet, Bel-Art) followed by isopropanol (Fisher Scientific) for 10 min each. After drying with an air gun, substrates were UV-ozone (Procleaner Plus, Bioforce) treated for 20 min and were subsequently spin-coated with a 7.68 mg/ml solution of zinc acetate dihydrate (Sigma-Aldrich) in ethanol (Sigma-Aldrich) and heated at 150 °C for 5 min in air. After a second coat of zinc acetate dihydrate solution was deposited and annealed, a 15-nm zinc oxide layer was formed.[22] The

substrates were subsequently transferred into a N_2 filled glovebox. A blend of P3HT (OS2100, Plextronics) and PCBM (Solenne BV) (1:1 by weight) in ortho-dichlorobenzene (Sigma-Aldrich, anhydrous) was dissolved by stirring at 60 °C for 3 h in N_2. The solution was then deposited on the substrates by spin coating at 600 rpm for 1 min in an N_2 environment. By changing the concentration (8:8, 16:16, and 24:24 mg/ml P3HT:PCBM), film thicknesses of $d = 100$, 190, 400 nm, with variation of less than 10 nm were achieved and confirmed via profilometer measurements (Dektak 8, Veeco). The devices were left in a covered Petri dish to slow-dry overnight. A solution of PEDOT:PSS, which consisted of 70% volume PEDOT:PSS (Clevois P VP AI 4083, HC Starck), 30% isopropanol (Fisher Scientific), and 0.2% Dynol 604 surfactant (Air Products), was spin coated on top of the P3HT:PCBM layer at 2000 rpm for 1 min in air to form a 50 nm hole transport layer. Then each device was annealed in N_2 atmosphere at 120 °C for 10 min. Finally, 100-nm of Ag was deposited through a shadow mask via thermal evaporation (Angstrom Engineering) under vacuum ($<10^{-7}$ Torr). The final devices contain 6 diodes with an active area of 0.11 cm^2 each. The schematic of the inverted device is shown in Figure 1 inset. For the 350-nm thick conventional device, a blend of 25:25 mg/ml P3HT (RMI-001E, Rieke Metals):PCBM in chlorobenzene (Sigma-Aldrich, anhydrous) was dissolved by stirring for 14 hours at 60 °C in N_2. The solution was spin coated at 400 rpm for 1 min, and the film was annealed in N_2 at 170 °C for 10 min. A 10-nm thick Ca and 100-nm thick Al were thermally evaporated through a shadow mask to complete the device.

B. *JV* characterization

JV measurements were collected under illumination from a class ACB[23] solar simulator (Oriel 67005) with an AM1.5G filter,[24] and the photocurrent was measured in nitrogen using a low noise sourcemeter (2635A, Keithley) controlled by LabView (National Instruments). The solar simulator intensity was set to 100 mW/cm^2 using a NREL-calibrated Si photodiode, and was attenuated down to 1 mW/cm^2 by inserting a set of neutral density filters (Newport, FSQ-ND series). These
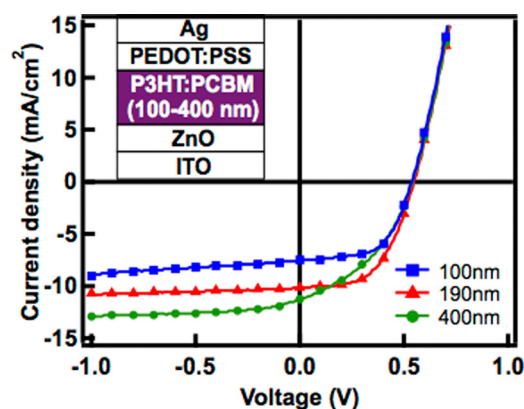
FIG. 1. *JV* curves taken at AM 1.5G one-sun (100 mW/cm^2) illumination conditions of inverted P3HT:PCBM BHJ solar cells with different active layer thicknesses: 100 nm (blue squares), 190 nm (red triangles), and 400 nm (green circles). (Inset) Schematic of the inverted device structure.

metallic neutral density filters have less than 8% variation in transmittance according to the manufacturer. Using the NREL calibrated Si-photodiode reference cell, we estimate a <5% spectral error, thus roughly <0.4% overall error on intensity measurements. The current-voltage (JV) curves of these devices taken in the solar simulator at one sun show that thicker active layer (190 nm and 400 nm) devices produce higher J_{sc} (Figure 1 and Table I) than the thin active layer (100 nm) devices. However, going from 190 to 400 nm, the absorption (Figure S1) continues to increase but J_{sc} saturates, indicating that the increase in light absorption does not lead to correspondingly higher collected photocurrent under short-circuit conditions. JV curves taken at different intensities are given in Figure 4 and S2.

C. White-light biased EQE measurement

In an EQE experiment (Figure 2(a)), the output of a tungsten lamp (OSRAM) is tuned from 350 nm to 750 nm with a monochromator (Horiba TRIAX-180, grating 600 groove/mm), with a wavelength window of 3.53 nm. The monochromatic illumination intensity is typically in the nanowatt regime ($\sim 10^{-4}$–10^{-3} mW/cm^2). The intensity is measured using an NREL calibrated silicon photodiode (Hamamatsu, S2386-44 K). A chopper (Tetrahertz, C-995) and lock-in amplifier (Stanford Research System, SR830) are employed to increase the measurement sensitivity of the low-intensity modulated photocurrent signal. The modulated frequency was chosen to be 1959 Hz to improve signal-to-noise ratio since the noise floor and interference peaks due to 60 Hz and harmonics are much higher with white-light bias. A gooseneck lamp (Dolan-Jenner Industry, Fiber-Lite MI 150) is employed for continuous illumination as a background white-light bias. The intensity of this background light is varied from 1 to 100 mW/cm^2 (0.01–1 sun) using a set of neutral density filters (Newport FSQ-ND series). By scanning the monochromator across the wavelength range (350–750 nm), a spectrum of the differential current, $J_{LID}(\lambda, I, V)$, is obtained via lock-in detection.

D. TMM modeling

The exciton generation rate profile within the active layer is modeled using the 1D transfer matrix method[19,20] as implemented by the McGehee group at Stanford University.[25,26] The photovoltaic device is treated as a multilayer stack interacting with a planar wave of light incident normal to the substrate. For all materials, default optical constants of materials as provided by the McGehee group were used, except in the case of sol-gel ZnO, where constant values of n (1.8) and k (0) were used for all wavelengths. Absorption as a function

of wavelength at each position within the active layer was first calculated, then integrated with the AM1.5G spectral intensity to yield the exciton generation rate at each position. To examine the deviation of spectrally resolved α from its average value, two exciton generation rate profiles for the inverted device were calculated, corresponding to wavelength ranges of 450–600 nm and 600–750 nm. For the conventional device, exciton generation rate profiles were calculated for wavelength ranges of 450–570 nm and 570–750 nm (see Sec. VI).

III. INTENSITY-DEPENDENT PHOTOCURRENT RESPONSIVITY

In EQE measurements of photodiodes with a given responsivity, current density generated by photons of a given wavelength (λ) under background light bias intensity (I) and voltage bias (V), $J(\lambda, I, V)$, is obtained by summing the solar cell responsivity at each wavelength generated by AM1.5G light, $s(\lambda, I, V)$, using the following equation:

$$J(\lambda, I, V) = \int_\lambda \Phi_P(\lambda) \, s(\lambda, I, V) \, d\lambda, \tag{1}$$

where Φ_P is the spectral irradiance of the AM1.5G one-sun solar spectrum (W/cm^2/nm), and the absolute spectral response (A/W) of the test cell is $s(\lambda, I, V) = (q\lambda/hc)\eta_{EQE}$. Photon-to-electron conversion efficiency, η_{EQE}, quantifies the ratio of electrons collected in an external circuit to photons incident onto a photodiode, and by definition measures loss in the conversion process: $\eta_{EQE} = \eta_{Abs}\eta_{CS}\eta_{CC}$, where η_{Abs} is the absorption efficiency of incident photons, η_{CS} is the efficiency of charge separation of primary excitations, and η_{CC} is the efficiency of collection of charge-separated carriers.

In an EQE measurement system, the photocurrent generated at a specific wavelength, $J(\lambda, I, V)$, is normally measured under short circuit conditions ($V = 0$). As illustrated in Figure 2(b), EQE via chopped light/lock-in detection (LID) measures the carriers produced from the small perturbation on top of carriers produced by steady-state illumination conditions. Hence, it measures differential current or differential spectral responsivity, DSR,[27,28] not spectral responsivity, s, as typically thought. In general, the dependence of photocurrent on incident light intensity is described as

$$J(\lambda, I, V) = s(\lambda, I, V)I. \tag{2}$$

Here, we do not assume that s is independent of I. For organic photovoltaic cells, it is common to approximate Eq. (2) by $J = AI^\alpha = (A'I^{\alpha-1})I$, where the last step explicitly

TABLE I. Device parameters of inverted OPV devices with different P3HT:PCBM BHJ active layer thickness taken under AM 1.5G one-sun (100 mW/cm^2) illumination conditions using a solar simulator. The series resistances for all devices are the same, 9±1 Ω cm^2.

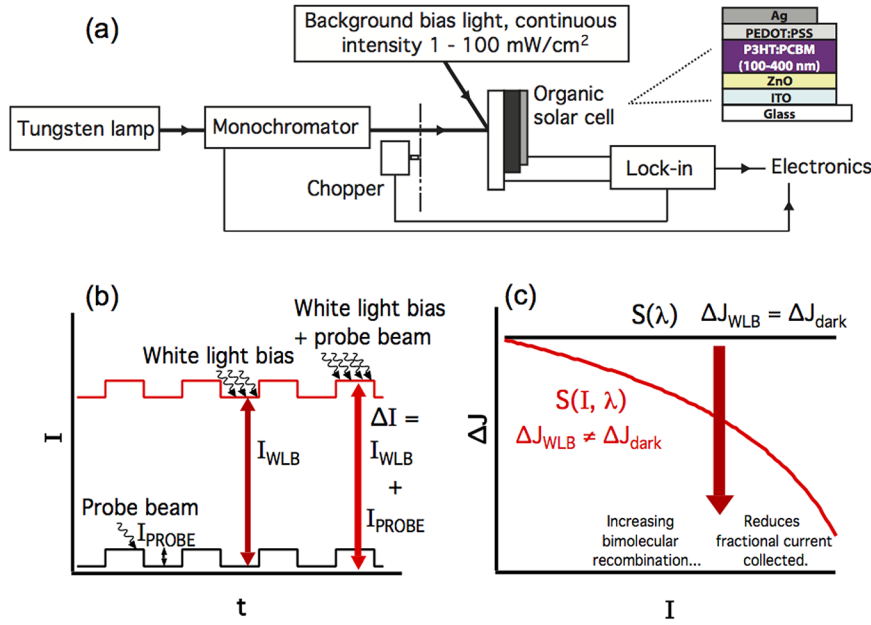| BHJ thickness	V_{oc} (V)	J_{sc} (mA cm^{-2})	FF	Eff (%)	R_{sh} (kΩ cm^2)
100 nm	0.54 ± 0.01	8.97 ± 0.61	0.58 ± 0.01	2.78 ± 0.18	6.6 ± 2.3
190 nm	0.56 ± 0.00	11.40 ± 0.77	0.52 ± 0.01	3.34 ± 0.19	192 ± 59
400 nm	0.54 ± 0.00	11.39 ± 0.29	0.40 ± 0.01	2.49 ± 0.04	168 ± 28

FIG. 2. (a) Experimental schematic of white-light biased external quantum efficiency measurement with monochromatic light of wavelength from 350 nm and 750 nm. (b) Schematic of optical excitation under white-light biased conditions, where a monochromatic intensity perturbation probes differential current generation under continuous white-light illumination. (c) Illustration of differential current as a function of white-light intensity for the case where spectral responsivity is linear (black) and sub-linear (red) in intensity.

shows the intensity dependence of s.[27] By differentiating Eq. (2) at constant voltage with respect to intensity, we see that $DSR = dJ(\lambda,I)/dI = s(\lambda,I) + Ids(\lambda,I)/dI$, and the assumption that $DSR = s$ is true only in the special case when $ds(\lambda,I)/dI = 0$, where current measured is linearly proportional to incident photons (Fig. 2(c) black). When J is not linear with I, i.e., $s(\lambda,I)$ is intensity dependent and $\alpha < 1$ (Fig. 2(c) red), care is required to obtain s from DSR measured via lock-in detection.[27–29]

Specifically, J obtained from EQE measurement via LID must be integrated to quantitatively compare to the photocurrent measured under one-sun, steady-state illumination (DSR $\rightarrow$ s). Below the detailed procedure is given for white-light biased EQE measurements taken at different background intensities. The current density at a given background light intensity (I_n) is obtained from EQE measurements by summing (integrating) the photocurrent density at each wavelength generated by modulated monochromatic light with correction for spectral mismatch between the monochromatic excitation light and the solar spectrum for a discrete number of measurements in background light intensity

$$J^*(I_n) \cong \sum_\lambda J^*(\lambda,I_n)\frac{\Phi_P(\lambda)}{\Phi_{mono}(\lambda)}$$

$$= \sum_\lambda \frac{J_{LID}(\lambda,I_0)I_0 + \sum_{i=1}^{n} J_{LID}(\lambda,I_i)(I_i - I_{i-1})}{I_n}$$

$$\times \frac{\Phi_P(\lambda)}{\Phi_{mono}(\lambda)}, \qquad (3)$$

where $i = 0, 1, 2,\ldots,$ to n measurements from low to high white-light bias, I_i, preferably including ~AM1.5G one-sun illumination and to low enough incident light intensity such that $d^2J/dI^2 \approx 0$.[29] In this paper, we use superscript * to indicate when the summation over intensity to convert DSR to s has been done. The photocurrent density is integrated over all wavelengths from the EQE spectrum. In Eq. (3), $\Phi_P(\lambda)$

and $\Phi_{mono}(\lambda)$ are the spectral irradiance of AM1.5G one-sun (W/cm^2/nm) and the monochromatic probe beam at the corresponding wavelength, respectively; $\Phi_P(\lambda)$ is obtained from NREL[24] and $\Phi_{mono}(\lambda)$ ($= J_{mono}(\lambda)/s_{mono}(\lambda)$) is measured using a calibrated silicon photodiode. Due to the discretized steps in incident light intensity, $J^*(I_i)$ at the lowest light intensity ($i = 0$) must be treated as a special case. In our measurement, $I_0 = 0$ (dark), so that the first term does not contribute. In the limit where responsivity is linear in intensity, i.e., $J_{LID}(\lambda, I_i) = J_{LID}(\lambda, I_{i-1})$, $J^*(\lambda, I_n)$ is the same as $J_{LID}(\lambda, I_n)$, as expected. $J^*(I_n)$ obtained in Eq. (3) approximates short circuit current measured in a solar simulator at the same excitation intensity regardless of whether s depends on I or not.

In Figure 3, we demonstrate the utility of integrating LID current to obtain an estimate of steady-state current density. Figure 3(a) depicts the spectral dependence of $J_{LID}(\lambda)$ (red squares) obtained from the lock-in signal directly and $J^*(\lambda)$ (blue triangles) obtained from the integration procedure outlined above for the 400 nm active layer device under one-sun white-light bias. Both J_{LID} and J^* in the figure have been corrected for the mismatch between the tungsten lamp and the AM 1.5G spectra. As is evident, the lock-in output underestimates J_{sc} at steady-state. This effect is distinctive of the case when J vs. I in Eq. (2) is sub-linear, i.e., $\alpha < 1$.[27] Indeed, the 400 nm solar cells demonstrate sub-linear intensity dependence even in steady-state (Figure S3). Short circuit current density J_{sc} vs. I of the $d = 400$ nm solar cell plotted in Figure 3(b) shows the current density determined (1) via steady-state JV measurements under different illumination from 1 to 100 mW/cm^2 (0.01–1 sun), $J_{sc}(JV)$, (black circles) (2) J_{LID}, calculated from simple integration of $J_{LID}(\lambda, I)$ in Figure 3(a) with respect to λ, (red squares) and (3) J^* obtained from $J^*(\lambda)$ in Figure 3(a) as outlined Equation (3) (blue triangles). The three methods for determining J_{sc} measure similar current density from 1 mW/cm^2 white-light bias to 30 mW/cm^2. In this regime, the response is roughly linear, i.e., $dJ/dI \sim s$, and $ds/dI \sim 0$. Above
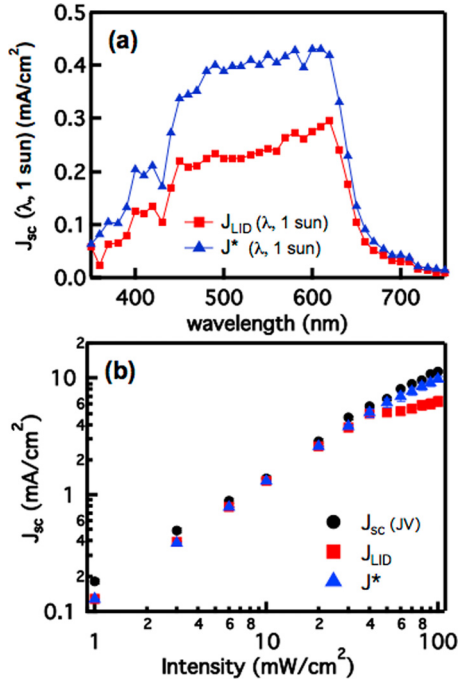
FIG. 3. (a) Spectral mismatch corrected $J_{LID}(\lambda)$ and $J^*(\lambda)$ of the $d = 400\,nm$ devices measured in the white-light biased EQE with background intensity of one sun. (b) J_{sc} vs. light intensity as measured at $V = 0\,V$ from JV measurements ($J_{sc}(JV)$, black circles), via lock-in detection (J_{LID}, red squares), and integrated lock-in signal (J^*, blue triangles) for the $d = 400\,nm$ device.

$30\,mW/cm^2$, response becomes nonlinear, and deviation between $J_{sc}(JV)$ and J_{LID} is clearly observable. In this regime, J_{LID} scales with DSR while $J_{sc}(JV)$ scales with s. By performing the integration procedure outlined in Eq. (3), we show that J^* is within 13% of $J_{sc}(JV)$ at $100\,mW/cm^2$: $9.8 \pm 0.6\,mA/cm^2$ vs. $11.3 \pm 0.3\,mA/cm^2$ measured at steady state. Increasing the number of white-light bias intensity steps in the EQE measurements will improve the agreement between the two results.

IV. MEASUREMENT OF RECOMBINATION FROM WHITE-LIGHT-BIASED EQE

In the EQE measurement, J^* is evaluated from the differential density of photogenerated carriers transported across the device as compared to background density of photogenerated carriers under no probe beam. Reduction in J^* with white-light bias compared to no white-light bias can therefore be interpreted as fractional loss of carriers due to the increased carrier density (Figure 2(b)). Hence, this method can be used to probe the dependence of recombination on background intensity, and is more sensitive than steady-state intensity-dependent current measurements because the high modulation frequency of the LID significantly reduces the noise contributions from slowly varying processes (e.g., temperature variation, amplifier gain drift, etc.) on the detected photocurrent. Assuming that reduction of collected charge carriers is entirely due to recombination and that intensity-dependent recombination is primarily bimolecular in nature,[9,30] bimolecular recombination efficiency (η_{BR}) at different light intensities can be defined as

$$\eta_{BR}(I) = 1 - \frac{J^*(I)}{J^*_{max}}, \qquad (4)$$

where J^*_{max} is the maximum of J^* for all intensities. Furthermore, the recombination parameter calculated from EQE (α_{EQE*}) and η_{BR} is related by[18]

$$\alpha_{EQE*} = (\eta_{BR} + 1)^{-1}. \qquad (5)$$

Thus, from EQE measurements at varying intensities of background white-light, we determine the recombination parameter, α_{EQE*}, as a function of excitation (incident light) intensity. No bimolecular recombination loss corresponds to η_{BR} of 0 and $\alpha_{EQE*} = 1$, while dominant bimolecular recombination is represented by η_{BR} of 1 and $\alpha_{EQE*} = 0.5$. When α_{EQE*} (intensity-dependent) is compared to α calculated from intensity-dependent JV measurements (α_{JV}, intensity averaged), we find that α_{EQE*} quantifiably correlates well with FF in the device measurements while α_{JV} does not.

V. NONLINEAR RESPONSIVITY IN INVERTED P3HT:PCBM SOLAR CELLS

To illustrate how white-light biased EQE can be used to measure bimolecular recombination, we examine inverted organic solar cells with different thicknesses of P3HT:PCBM bulk heterojunction (BHJ) active layer. Figures 4(a), 4(c), and 4(e) show EQE* spectra for the 100 nm, 190 nm, and 400 nm devices, respectively, under different white-light bias intensities. As can be seen from the plots, the EQE* spectra of the device with a thin active layer are independent of the intensity of the background white-light bias. In contrast, for devices with a thick active layer, the EQE* spectra are affected greatly by the background intensity, whereby the EQE* curves become more "flat" as the white-light bias intensity approaches one-sun. Hence, J^* calculated from Eq. (3) is independent of I for the 100 nm active layer device but decreases at high intensity for both the 190 nm and 400 nm active layer devices, indicating increased recombination losses in thicker active layers at high illumination intensities. Similar reduction in EQE signal and spectral changes under white-light illumination have been reported by Brenner *et al.* but were not analyzed in terms of recombination.[31,32]

Figures 4(b), 4(d), and 4(f) show steady-state JV spectra of the same devices taken under varying excitation intensity. For the d = 100 nm and d = 190 nm devices, reverse bias JV curves taken at different intensities can be scaled and are roughly independent of applied voltage up to maximum power point (MPP, marked as x in Figures 4(b), 4(d), and 4(f)), indicating monomolecular recombination.[2] However, the high-intensity JV curves of the $d = 400\,nm$ device, which shows the greatest non-linear spectral responsivity in EQE, exhibit a voltage dependence even at short circuit (Fig. 4(f)). This is consistent with the illumination intensity dependence of FF (Figure S2(d)). For the $d = 400\,nm$ device, FF is reduced dramatically at high intensity. Measurement of the recombination in these devices via EQE quantifies the recombination loss qualitatively observed in the JV data, which is not easily observed under steady-state short-circuit conditions.
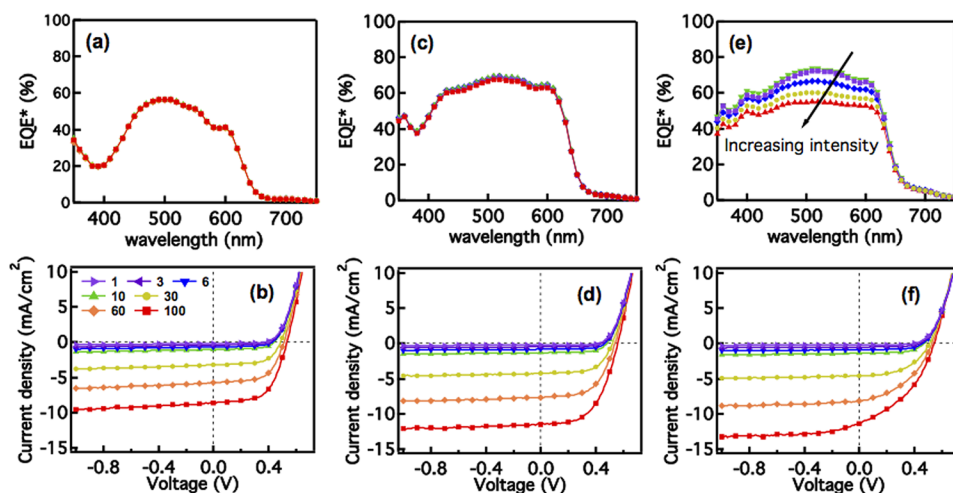
FIG. 4. The EQE* and *JV* spectra taken under different intensities of white-light bias on inverted P3HT:PCBM devices with active layer thickness of (a) and (b) 100 nm, (c) and (d) 190 nm, and (e) and (f) 400 nm. Background light intensities are 1 mW/cm^2 (light purple right-facing triangles), 3 mW/cm^2 (dark purple left-facing triangles), 6 mW/cm^2 (blue upside down triangles), 10 mW/cm^2 (green triangles), 30 mW/cm^2 (yellow circles), 60 mW/cm^2 (orange diamonds), and 100 mW/cm^2 (red squares). In all, lines are guides to the eye, *JV* data shown in (b), (d), (f) are a subset of a larger set of data taken, abbreviated here for clarity and shown in full in Figure S2.

By normalizing to J^*_{max} for each device (Eq. (4)), we obtain η_{BR} vs. *I*. Using Eq. (5) to convert η_{BR} to α_{EQE*}, Figure 5 shows the white-light intensity dependence of α_{EQE*} for the three thicknesses of inverted P3HT:PCBM BHJ solar cells. For the 100 nm active layer devices (blue squares), $\alpha_{EQE*} \sim 1$ across all intensities, indicating low bimolecular recombination at all intensities. The corresponding *FF* of the *JV* curve at one-sun remains high (*FF* = 0.58). α_{EQE*} starts to deviate from unity at 50 mW/cm^2 for devices with d = 190 nm active layer (red triangles) and at 30 mW/cm^2 for the 400 nm active layer (green circles) devices, implying that bimolecular recombination plays an important role in these thicker devices when high background carrier densities and/or reduced internal field is present. In particular, $\alpha_{EQE*} = 0.80 \pm 0.03$ at 100 mW/cm^2 for the 400 nm thick devices, consistent with the low *FF* value of 0.40. At 1 mW/cm^2, the 400 nm active layer devices exhibit a *FF* value (*FF* = 0.60) that is comparable to *FF* of the 100 nm active layer devices because at this low intensity (carrier density), bimolecular recombination plays a minimal role. The dependence of the recombination parameter α_{EQE*} on *I* (Figure 5) demonstrates that white-light biased EQE measurements are able to quantify intensity-dependent recombination effects under short-circuit conditions. While not the main focus of this paper, it is interesting to note that both α_{EQE*} in Fig. 5 and *FF* in Figure S2(d) also decrease at

low illumination intensity (<10 mW/cm^2). This behavior is consistent with reduced charge collection due to recombination through a fixed density of unoccupied sub-gap states, which can be filled with increasing intensity. These unoccupied states could be the tail states in the active layer,[33–35] trap states in ZnO layer,[36] or at the interfaces between two layers.[37,38]

To further demonstrate the relationship between the recombination parameter determined from white-light biased EQE measurements and fill factor from *JV* measurements, α_{EQE*} (d = 400 nm) is plotted vs. intensity-dependent *FF* in Figure 6(a) (also see Figure S4). Evidence presented here supports the hypothesis that white-light biased EQE directly
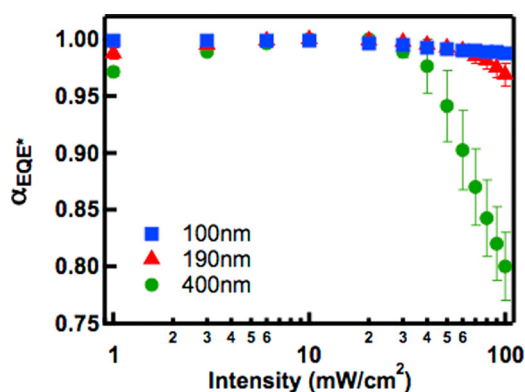

FIG. 5. Light-intensity dependent α_{EQE*} as derived from EQE measurements for the P3HT:PCBM BHJ inverted architecture devices with active layer thicknesses, d = 100 nm (blue squares), d = 190 nm (red triangles), and d = 400 nm (green circles).
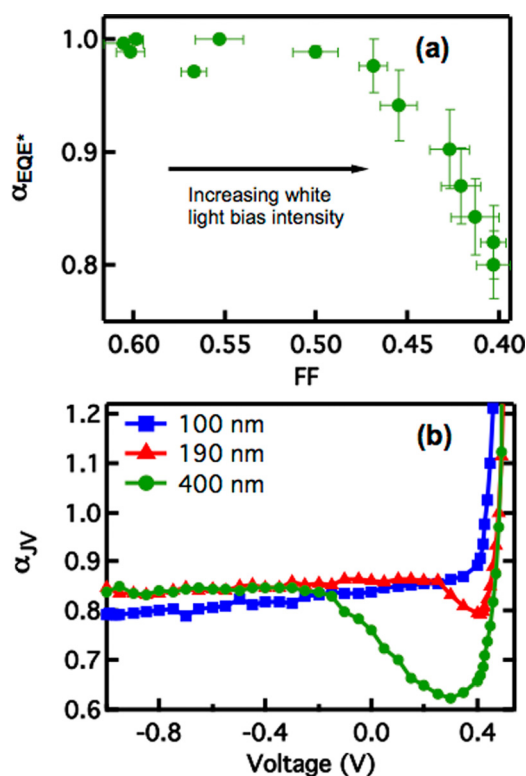
FIG. 6. (a) α_{EQE*} plotted versus intensity-dependent fill factor extracted from *JV* for the d = 400 nm P3HT:PCBM BHJ inverted architecture device; (b) Voltage-dependent α_{JV} extracted from *JV* measurements (power law fit to data from 30 to 100 mW/cm^2 illumination intensity).

probes the bimolecular recombination responsible for reduced FF in these OPV devices.

In contrast, the recombination parameter, α_{JV}, can be obtained from JV curves in the solar simulator with different illumination intensities. Figure 6(b) shows α_{JV} power law fitted from steady-state JV curves measured at intensity range $I = 30$–$100 \, \text{mW/cm}^2$ and for voltage range $-1.0 \, \text{V} < V < 0.5 \, \text{V}$. α_{JV} shows clear voltage dependence for the $d = 100$, 190, and 400 nm solar cells. The α_{JV} values do not differ significantly for all devices at reverse bias ($-1.0 \, \text{V} < \text{V} < 0 \, \text{V}$). In this regime, α_{JV} deviates from unity similarly for the three devices, which suggests similar recombination loss in the three devices at reverse bias conditions, consistent with previous observations of efficient sweep-out of carriers in reverse bias.[39,40] Above $V = 0 \, \text{V}$ and nearing $+0.3 \, \text{V}$ bias (Figure 6(b)), α_{JV} decreases for the 190-nm and 400-nm devices. The decrease in α_{JV} near the maximum power point appears correlated to reduced fill factor at high intensity observed in Figure 6(a). Nearing open circuit, α_{JV} increases significantly due to increased diffusion current contribution and dark diode current injection. However, the exact numerical value of α_{JV} depends on the choice of bias and the range of intensities used for the fitting (also see Figure S5). Thus, the use of an intensity-averaged measurement of intensity-dependent recombination is qualitatively informative but fundamentally flawed. In contrast, white-light biased EQE measurements enable one to probe the intensity-dependent recombination processes that contribute to reduced FF and overall device performance.

VI. SPECTRALLY DEPENDENT RESPONSIVITY AND RECOMBINATION

EQE measurements performed in this study include spectrally resolved data across the P3HT:PCBM absorption spectrum ($\lambda = 350$–$750 \, \text{nm}$), and analysis of the wavelength dependence of α_{EQE*} provides insight into the source of increased bimolecular recombination in the bulk heterojunction. We analyze wavelength dependence of α_{EQE*}, in contrast to previous measurements which were done at a single wavelength.[18] Figure 7(a) shows α_{EQE*} vs. λ from 350 to 750 nm (black triangles), in addition to the full-spectrum value that is determined from Eq. (5) (black line), for the 400-nm active layer inverted device under $100 \, \text{mW/cm}^2$ background illumination. Recombination is clearly wavelength dependent; in particular, α_{EQE*} is lower (higher recombination) where P3HT absorbs strongly, $\lambda \sim 450$ to 600 nm, and higher (lower recombination) for $\lambda \geq 600 \, \text{nm}$ (carriers produced in response to photons absorbed near or below the band gap). To determine the cause for the wavelength dependence, we simulated the optical field distribution in the device using 1D transfer matrix method (TMM), which has been shown to effectively model absorption in organic photovoltaic devices.[19,20,25] The optical field distribution is then integrated with AM1.5G spectral intensity data over the two wavelength ranges to calculate the exciton generation rate profiles. Most of the excitons from 450 to 600 nm photons are generated near the front contact of the inverted solar cells—i.e., the ZnO-coated ITO (electron
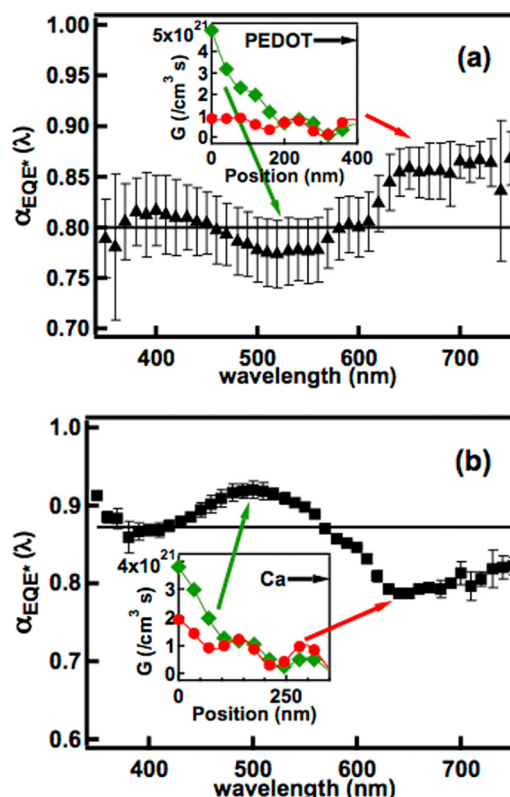

FIG. 7. Wavelength dependence of α_{EQE*} between 350 to 750 nm at $100 \, \text{mW/cm}^2$ illumination intensity (triangles) for **(a)** 400-nm active layer inverted devices and (b) 350-nm active layer conventional devices. The solid black line represents α_{EQE*} calculated from J^*, i.e., full-spectrum value. Inset: Exciton generation rate profiles calculated using TMM in the active layer for (a) 450–600 nm wavelength regime (green diamonds) and 600–750 nm regime (red) in the inverted device structure, and (b) 450–570 nm wavelength regime (green) and 570–750 nm regime (red circles) for 350-nm thick conventional devices. 0 nm in the position represents the interface between the front contact (ZnO in (a) and PEDOT in (b)) and the active layer, and maximum position represents interface between the active layer and the back contact (PEDOT in (a) and Ca in (b)).

collection layer), while excitons generated from longer wavelength photons occur more uniformly across the thickness of the P3HT:PCBM active layer (Figure 7(a) inset). Due to the short exciton diffusion length ($\sim$10 nm), the hole and electron generation rate profiles should be similar to the exciton generation rate profile. Since the front contact (ITO/ZnO) collects electrons and the back contact (PEDOT:PSS/Ag) collects holes in an inverted architecture, the spectral dependence of α_{EQE*} in the inverted device is consistent with lower hole mobility[3,18] being the culprit for inefficient charge collection.[32] Specifically, higher recombination (lower α_{EQE*}) is observed for the wavelength range where holes must traverse a longer distance on average than electrons before collection.

To test this hypothesis, we examine a thick (350-nm) conventional device with P3HT:PCBM BHJ active layer, in which the front contact (ITO/PEDOT:PSS) collects the holes and the back contact (Ca/Al) collects the electrons (Figure 7(b)). The spectral dependence of α_{EQE*} for this conventional device shows the opposite trend: α_{EQE*} is higher between 450 and 570 nm and lower for $\lambda \geq 570 \, \text{nm}$. The generation rate profiles for the conventional device are qualitatively similar to those

for the inverted device. However, since the holes are collected at the front contact and electrons are collected at the back contact, this device exhibits more efficient charge collection when holes are generated near the front contact, i.e., near P3HT absorption maximum. Moreover, the full-spectrum α_{EQE*} value of the conventional device (Figure 7(b), solid black line) is higher than that of the inverted devices (Figure 7(a), solid black line), which is again consistent with lower hole mobility compared to electron mobility. Another possible contributing factor to increased recombination in the thick P3HT:PCBM devices studied here is the larger work function difference between the charge transport layers in the conventional device (PEDOT:PSS and Ca) compared to the inverted devices (ZnO and PEDOT:PSS), which decreases the spatial extent of the field-free region arising from screening of the built-in field by background charges,[41] thus increasing charge collection efficiency and decreasing recombination. Nevertheless, the wavelength dependence of α_{EQE*} gives useful insight on the relationship between carrier generation and collection in OPVs.

In work published recently by Koster *et al.*,[18] the recombination parameter, α, is evaluated under single-wavelength excitation. We assert that measurement at a single wavelength cannot be generalized to assess overall bimolecular recombination in an organic solar cell, due in part to the spectral dependence of bimolecular recombination. While the approach of integrating EQE* spectra (Eq. (3) presented in this paper) appears to be a simple extension of the approach of Koster *et al.*, it has profound implications to measurement of recombination parameter. Integrating over the entire absorption region of the cell's active materials produces a single recombination parameter (full-spectrum α_{EQE*}) representative of the device response at particular illumination intensity more accurately representing AM1.5G illumination conditions. As shown in Figure 6(a) and Figure S4, α_{EQE*} values determined by this method correlate well with device *FF*. While it is possible to obtain a spectrally averaged α_{EQE*} from single-wavelength measurements at several selected wavelengths, the average value $\langle \alpha_{EQE*}(\lambda) \rangle$ obtained from this approach will depend on the selection of the wavelengths and intervals between data points. As Figure 7(a) shows for inverted cells, if more data points were sampled between 450 and 600 nm than outside of this wavelength range, $\langle \alpha_{EQE*}(\lambda) \rangle$ would artificially decrease, leading to inflated values for recombination. The opposite would occur for the conventional devices tested in Figure 7(b). To illustrate this point, Figure S6(a) plots the same data shown in Figure 7(a), while Figure S6(b) is a reduced data set with data points at 30 nm intervals for $\lambda > 600$ nm. For the data set in Figure S6(a), the full-spectrum $\alpha_{EQE*} = 0.80 \pm 0.03$ (calculated from the integrated current), while $\langle \alpha_{EQE*}(\lambda) \rangle$ (calculated from averaging $\alpha_{EQE*}(\lambda)$ at every wavelength) $= 0.82 \pm 0.03$, indicating lower recombination. For the data set in Figure S6(b), the full-spectrum value remains the same while $\langle \alpha_{EQE*}(\lambda) \rangle$ is now reduced, approaching α_{EQE*}. This analysis artifact follows from assuming that α at each wavelength contributes equally to total recombination, an incorrect assumption when the concentration and distribution of photogenerated carriers vary significantly at different

wavelengths, as shown in Figure 7(a) inset. While the difference shown in this example is not large, it is possible that the discrepancy could be much larger in other cases. Integrating the EQE* spectrum to obtain J^* before calculating α_{EQE*} is a more robust determination of recombination parameter. The integrated J^* does not depend strongly on sampling frequency as long as enough wavelengths are sampled to form an accurate spectrum. Thus, the approach presented in this paper, i.e., calculating the recombination parameter, α, via integrated J^*, is more physically representative of relevant recombination in devices than evaluating $\alpha(\lambda, I)$ at single wavelengths and then averaging.

VII. CONCLUSION

In summary, we demonstrate the use of white-light biased differential current measurement (EQE) to quantify intensity-dependent (bimolecular) recombination as a function of wavelength and carrier density as varied via total incident illumination intensity. Non-linearity in the responsivity to intensity variation can lead to significant discrepancies between J_{LID} and $J_{sc}(JV)$ at high illumination (30–100 mW/cm^2) for devices with high bimolecular recombination. However, we confirm that integrating measured LID current values produces comparable current values between EQE and *JV* results. We show that recombination parameter, α_{EQE*}, values determined via this approach accurately reflect device *FF* in steady-state *JV* measurements. The close relationship between increased intensity-dependent recombination and reduced *FF* likely results from a decrease in the internal field in the device near the maximum power point, and can be accentuated by increasing active layer thickness and carrier density (proportional to incident illumination intensity). From the spectral dependence of recombination efficiency and TMM simulations, we attribute increased recombination in thick (350–400 nm) active layer devices to a spatially non-uniform distribution of carrier generation across the active layer thickness. Lastly, since an EQE setup is ubiquitous in research laboratories, the white-light biased EQE can be easily adapted as a useful tool to probe photon-to-electron conversion loss in OPV systems. Studies investigating mechanisms impacting recombination rates in OPV devices, including contact layer performance, different donor-acceptor combinations, and donor-acceptor morphology are in progress.

ACKNOWLEDGMENTS

[1]L. J. A. Koster, V. D. Mihailetchi, and P. W. M. Blom, Appl. Phys. Lett. **88**, 052104 (2006).

[2]S. R. Cowan, A. Roy, and A. J. Heeger, Phys. Rev. B **82**, 245207 (2010).

[3]L. J. A. Koster, V. D. Mihailetchi, H. Xie, and P. W. M. Blom, Appl. Phys. Lett. **87**, 203502 (2005).

[4]W. Tress, K. Leo, and M. Riede, Phys. Rev. B **85**, 155201 (2012).

[5]Z. M. Beiley, E. T. Hoke, R. Noriega, J. Dacuña, G. F. Burkhard, J. A. Bartelt, A. Salleo, M. F. Toney, and M. D. McGehee, Adv. Energy Mater. **1**, 954 (2011).

[6]J. C. Blakesley and D. Neher, Phys. Rev. B **84**, 075210 (2011).

[7]C. G. Shuttle, R. Hamilton, B. C. O'Regan, J. Nelson, and J. R. Durrant, Proc. Natl. Acad. Sci. U.S.A. **107**, 16448 (2010).

[8]V. D. Mihailetchi, J. Wildeman, and P. W. M. Blom, Phys. Rev. Lett. **94**, 126602 (2005).

[9]C. G. Shuttle, B. C. O'Regan, A. M. Ballantyne, J. Nelson, D. D. C. Bradley, and J. R. Durrant, Phys. Rev. B **78**, 113201 (2008).

[10]A. J. Mozer, N. S. Sariciftci, L. Lutsen, D. Vanderzande, R. Osterbacka, M. Westerling, and G. Juška, Appl. Phys. Lett. **86**, 112104 (2005).

[11]C. Deibel, A. Baumann, A. Wagenpfahl, and V. Dyakonov, Synth. Met. **159**, 2345 (2009).

[12]A. Pivrikas, G. Juška, A. J. Mozer, M. C. Scharber, K. Arlauskas, N. S. Sariciftci, H. Stubb, and R. Osterbacka, Phys. Rev. Lett. **94**, 176806 (2005).

[13]G. Sliauzys, G. Juška, K. Arlauskas, A. Pivrikas, R. Osterbacka, M. C. Scharber, A. J. Mozer, and N. S. Sariciftci, Thin Solid Films **511**, 224 (2006).

[14]P. Schilinsky, C. Waldauf, and C. J. Brabec, Appl. Phys. Lett. **81**, 3885 (2002).

[15]J. van Duren, X. Yang, J. Loos, C. Bulle-Lieuwma, A. B. Sieval, J. Hummelen, and R. A. J. Janssen, Adv. Funct. Mater. **14**, 425 (2004).

[16]I. Riedel, J. Parisi, V. Dyakonov, L. Lutsen, D. Vanderzande, and J. Hummelen, Adv. Funct. Mater. **14**, 38 (2004).

[17]D. Gebeyehu, M. Pfeiffer, B. Maennig, J. Drechsel, A. Werner, and K. Leo, Thin Solid Films **451**, 29 (2004).

[18]L. J. A. Koster, M. Kemerink, M. M. Wienk, K. Maturová, and R. A. J. Janssen, Adv. Mater. **23**, 1670 (2011).

[19]L. A. A. Pettersson, L. S. Roman, and O. Inganas, J. Appl. Phys. **86**, 487 (1999).

[20]P. Peumans, A. Yakimov, and S. R. Forrest, J. Appl. Phys. **93**, 3693 (2003).

[21]See supplementary material at http://dx.doi.org/10.1063/1.4801920 for absorption data, JV curves taken at all illumination intensities, illumination intensity dependence of short circuit current, correlation of recombination parameter with fill factor at 1 sun, differential analysis of intensity- and voltage-dependent *JV* data, and data for two different methods to obtain recombination parameter over the entire spectrum.

[22]Y.-J. Lee, R. J. Davis, M. T. Lloyd, P. P. Provencio, R. P. Prasankumar, and J. Hsu, IEEE J. Sel. Top. Quantum Electron. **16**, 1587 (2010).

[23]Standard International Electrotechnical Commission IEC 60904-9, Solar Simulator Performance Requirements, Geneva, Switzerland.

[24]See http://Rredc.Nrel.Gov/Solar/Spectra/am1.5/ (n.d.) for spectral irradiance of AM1.5G one-sun.

[25]G. F. Burkhard, E. T. Hoke, and M. D. McGehee, Adv. Mater. **22**, 3293 (2010).

[26]M. D. McGehee, "Transfer matrix optical modeling," can be found under http://www.stanford.edu/group/mcgehee/transfermatrix/ (n.d.).

[27]T. J. McMahon and K. Sadlon, Sol. Cells **13**, 99 (1984).

[28]J. Metzdorf, Appl. Opt. **26**, 1701 (1987).

[29]D. J. Wehenkel, K. H. Hendriks, M. M. Wienk, and R. A. J. Janssen, Org. Electron. **13**, 3284 (2012).

[30]A. Maurano, R. Hamilton, C. G. Shuttle, A. M. Ballantyne, J. Nelson, B. O'Regan, W. Zhang, I. Mcculloch, H. Azimi, M. Morana, C. J. Brabec, and J. R. Durrant, Adv. Mater. **22**, 4987 (2010).

[31]T. J. K. Brenner, H. Inchan, N. C. Greenham, and C. R. McNeill, J. Appl. Phys. **107**, 114501 (2010).

[32]T. J. K. Brenner, Y. Vaynzof, Z. Li, D. Kabra, R. H. Friend, and C. R. McNeill, J. Phys. D. Appl. Phys. **45**, 415101 (2012).

[33]G. Garcia-Belmonte and J. Bisquert, Appl. Phys. Lett. **96**, 113301 (2010).

[34]R. A. Street, Phys. Rev. B **84**, 075208 (2011).

[35]T. Kirchartz, B. E. Pieters, J. Kirkpatrick, U. Rau, and J. Nelson, Phys. Rev. B **83**, 115209 (2011).

[36]M. R. Lilliedal, A. J. Medford, M. V. Madsen, K. Norrman, and F. C. Krebs, Sol. Energy Mater. Sol. Cells **94**, 2018 (2010).

[37]B. T. de Villers, C. J. Tassone, S. H. Tolbert, and B. J. Schwartz, J. Phys. Chem. C **113**, 18978 (2009).

[38]A. Kumar, S. Sista, and Y. Yang, J. Appl. Phys. **105**, 094512 (2009).

[39]S. R. Cowan, R. A. Street, S. Cho, and A. J. Heeger, Phys. Rev. B **83**, 035205 (2011).

[40]N. S. Christ, S. W. Kettlitz, S. Valouch, S. Züfle, C. Gärtner, M. Punke, and U. Lemmer, J. Appl. Phys. **105**, 104513 (2009).

[41]A. J. Morfa, A. M. Nardes, S. E. Shaheen, N. Kopidakis, and J. Van De Lagemaat, Adv. Funct. Mater. **21**, 2580 (2011).